

ULRR

Structural phase transformations induced by guest molecules in a nickel-based 2D Square lattice coordination network

Item Type	Article
Authors	Li, Xia;Sensharma, Debobroto;Nikolayenko, Varvara Igorivna;Darwish, Shaza;Bezrukov, Andrey;Kumar, Naveen;Liu, Wansheng;Kong, Xiang-Jing;Zhang, Zhenjie;Zaworotko, Michael
Citation	Chemistry of Materials, 2023, 35,pp. 783-791
Publisher	American Chemical Society
Download date	2026-06-10 12:08:27
Item License	https://creativecommons.org/licenses/by-nc-sa/4.0/
Link to Item	https://doi.org/10.34961/researchrepository-ul.23622894

Structural Phase Transformations Induced by Guest Molecules in a Nickel-Based 2D Square Lattice Coordination Network

Xia Li, Debobroto Sensharma, Varvara I. Nikolayenko, Shaza Darwish, Andrey A. Bezrukov, Naveen Kumar, Wansheng Liu, Xiang-Jing Kong, Zhenjie Zhang, and Michael J. Zaworotko*



Cite This: *Chem. Mater.* 2023, 35, 783–791



Read Online

ACCESS |



Metrics & More

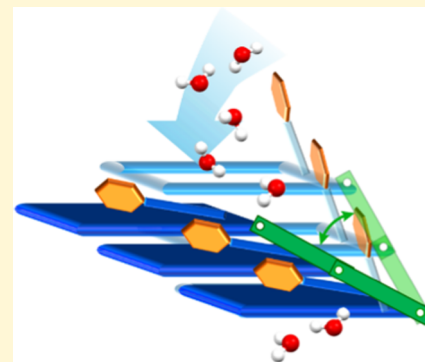


Article Recommendations



Supporting Information

ABSTRACT: Herein, we report the crystal structure and guest binding properties of a new two-dimensional (2D) square lattice (sql) topology coordination network, sql-(azpy)(pdia)-Ni, which is comprised of two linker ligands with diazene (azo) moieties, (*E*)-1,2-di(pyridin-4-yl)diazene (azpy) and (*E*)-5-(phenyldiazenyl)isophthallate (pdia). sql-(azpy)(pdia)-Ni underwent guest-induced switching between a closed (nonporous) β phase and several open (porous) α phases, but unlike the clay-like layer expansion to distinct phases previously reported in switching sql networks, a continuum of phases was formed. In effect, sql-(azpy)(pdia)-Ni exhibited elastic-like properties induced by adaptive guest binding. Single-crystal X-ray diffraction (SCXRD) studies of the α phases revealed that the structural transformations were enabled by the pendant phenyldiazenyl moiety on the pdia²⁻ ligand. This moiety functioned as a type of hinge to enable parallel slippage of layers and interlayer expansion for the following guests: *N,N*-dimethylformamide, water, dichloromethane, *para*-xylene, and ethylbenzene. The slippage angle (interplanar distances) ranged from 54.133° (4.442 Å) in the β phase to 69.497° (5.492 Å) in the ethylbenzene-included phase. Insight into the accompanying phase transformations was also gained from variable temperature powder XRD studies. Dynamic water vapor sorption studies revealed a stepped isotherm with little hysteresis that was reversible for at least 100 cycles. The isotherm step occurred at ca. 50% relative humidity (RH), the optimal RH value for humidity control.



both interpenetrated²⁵ and noninterpenetrated²⁶ variants. These sql networks are highly amenable to crystal engineering²⁷ thanks to their modularity in terms of the metal, linker ligands, and for octahedral metal centers, the terminal ligand.^{28–30} Our analysis of the TOPOS topological types observed database³¹ and Cambridge Structural Database³² (TOPOS TTO \cap CSD databases, see Supporting Information for details) revealed that there are >9000 sql network examples (Figure S1). Out of these, >2500 sql networks have been reported involving N-donor linker ligands, including both single-linker and mixed-linker sql networks.³³

INTRODUCTION

Since “third generation coordination polymers”¹ or “soft porous crystals”² were introduced in the late 1990s and early 2000s, flexible metal–organic materials (FMOMs), i.e., materials that adjust their structures when exposed to external stimuli, have been explored with emphasis upon their potential utility for gas, vapor, and liquid storage applications.^{3–7} Whereas rigid porous coordination networks (PCNs) typically display type I (Langmuir) sorption isotherms and some microporous PCNs can exhibit exceptional selectivity in the context of separation of industrially relevant gas and vapor mixtures, such as C1 gases;⁸ C2 gases;^{9,10} C3 gases;^{11,12} C6 aromatics;¹³ and C8 aromatics,¹⁴ FMOMs can undergo structural transformation(s) in response to guest molecules and sometimes exhibit sharp-stepped isotherms that are usually accompanied by a phase transformation from a closed (nonporous) to an open (porous) phase (switching).^{15–19} The ability of FMOMs to adjust their pore geometry as a consequence of structural transformations^{20–22} can enable enhanced working capacity and thermodynamic management, which is relevant for gas storage applications.²³

An archetypal class of PCNs is the family of coordination networks with square lattice (sql) topology, the prototypal variant of which was reported in 1970.²⁴ In the 1990s, sql networks involving 4,4'-bipyridine, bpy, were introduced with

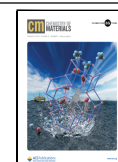
An interesting feature of sql networks is that when they form layered structures, they can exhibit switching transformations between closed and open phases. The structure of the prototypal switching sql network, [Cu(bpy)₂(BF₄)₂], ELM-11, was reported in 2001.³⁴ ELM-11^{35,36} and its variant, ELM-12,³⁰ [Cu(bpy)₂(OTf)₂], OTf = triflate, have been widely studied along with other bpy linked sql analogues.³⁷ More

Received: December 8, 2022
Revised: December 20, 2022
Published: January 10, 2023

Received: December 8, 2022

Revised: December 20, 2022

Published: January 10, 2023



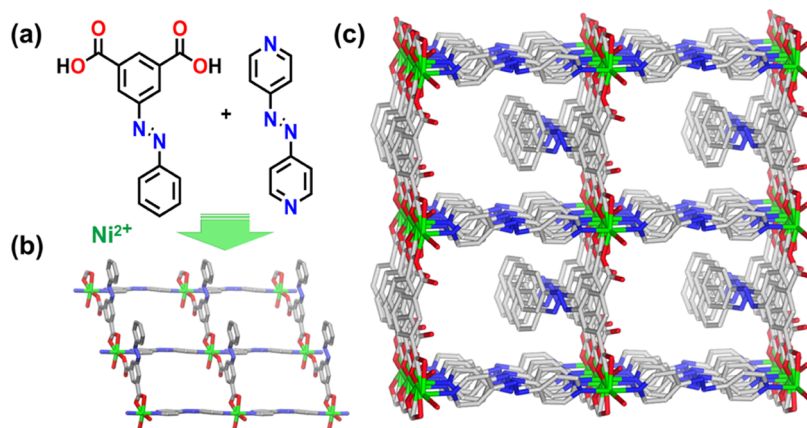


Figure 1. (a) Ligands (*E*)-5-(phenyldiazenyl) isophthalic acid (H_2pdia , left) and (*E*)-1,2-di(pyridin-4-yl)diazene (*azpy*, right). (b) **sqf** layer in **sqf-(azpy)(pdia)-Ni**. (c) One-dimensional (1D) channels lie along the *c*-axis in the as-synthesized form (disordered guests are omitted for the sake of clarity), **sqf-(azpy)(pdia)-Ni- α_{DMF}** .

recently, $[Co(bipy)_2(NCS)_2]$, **sqf-1-Co-NCS**, set a new performance benchmark for C8 hydrocarbon separations in terms of both selectivity and uptake.¹⁷ The mechanism of switching in such networks can be attributed to clay-like expansion/shrinkage between adjacent layers of **sqf** planes and typically results in distinct phases supported by interlayer interactions in addition to layer–guest interactions.^{28,38} Typically, there is little deformation or flexibility associated with the **sqf** network itself.

Ligands with diazene (azo) moieties are known to enable deformation and so offer the potential for additional flexibility.^{39–41} Thus far, only four structures have been reported based upon $H_2pdia = (E)$ -5-(phenyldiazenyl)-isophthalic acid, H_2pdia (Figure 1a), but these studies did not focus on sorption, and none were reported to be flexible.^{42,43} In TOPOS TTO \cap CSD databases, 55 **sqf** networks based upon (*E*)-1,2-di(pyridin-4-yl)diazene, *azpy* (Figure 1a) linkers have been reported (Figure S2 and Table S1), 26 of which are single-linker **sqf** nets (Type I-a),³³ whereas 19 examples are mixed-linker **sqf** nets with dicarboxylate anions as the second linker (Type II-ab).³³ Although **sqf** nets based on two distinct azo-bearing linkers⁴⁴ and flexible **sqf** nets featuring azo-functionality⁴⁵ have been studied, to the best of our knowledge, the flexibility of the diazene moiety has not been exploited to induce switching behavior.

In this study, we report what is to our knowledge, the first example of a switching **sqf** network sustained by mixed-linker ligands that both contain azo moieties, **sqf-(azpy)(pdia)-Ni** ($[Ni(pdia)(azpy)(H_2O)]$, Figure 1a), its unusual guest-induced switching behavior, and characterization of that switching behavior with emphasis upon the effect of the pendant azo moiety of the $pdia^{2-}$ linker ligand upon the nature of the observed structural changes.

EXPERIMENTAL SECTION

sqf-(azpy)(pdia)-Ni- α_{DMF} , $\{[Ni(azpy)(pdia)(H_2O)] \cdot DMF\}$. *Synthesis.* A mixture of $Ni(NO_3)_2 \cdot 6H_2O$ (0.15 mmol, 43.5 mg), (*E*)-1,2-di(pyridin-4-yl)diazene (*azpy*) (0.15 mmol, 27.6 mg), (*E*)-5-(phenyldiazenyl)isophthalic acid (H_2pdia) (0.15 mmol, 40.5 mg), *N,N*-dimethylformamide (DMF) (5.0 mL), and water (H_2O) (5.0 mL) was added to a 20 mL glass vial. The vial was capped tightly and placed in an oven at 105 °C for 24 h, which was then cooled to room temperature. After rinsing several times with fresh DMF, brown single

crystals were obtained. Yield: 78%. IR: ν_{max} (cm^{-1}) = 3392, 3292, 2934, 2868, 1650, 1596, 1524, 1388, 1219, 1096, 776, 718.

sqf-(azpy)(pdia)-Ni- β , $[Ni(azpy)(pdia)(H_2O)]$. *Synthesis.* The as-synthesized open framework (**sqf-(azpy)(pdia)-Ni- α_{DMF}**) was exchanged with fresh methanol (MeOH) using a Soxhlet extractor for 2 days and then heated to 100 °C under vacuum for 10 h to yield **sqf-(azpy)(pdia)-Ni- β** . IR: ν_{max} (cm^{-1}) = 3363, 1593, 1557, 1531, 1353, 1222, 1044, 1019, 918, 832, 761, 715.

sqf-(azpy)(pdia)-Ni- α_{H_2O} , $\{[Ni(azpy)(pdia)(H_2O)] \cdot 3H_2O\}$. *Synthesis.* The activated closed framework (**sqf-(azpy)(pdia)-Ni- β**) was soaked in water for 1 day to yield **sqf-(azpy)(pdia)-Ni- α_{H_2O}** . IR: ν_{max} (cm^{-1}) = 3326, 1596, 1553, 1530, 1356, 1222, 1144, 1099, 1050, 1015, 918, 778, 721, 684.

sqf-(azpy)(pdia)-Ni- α_{DCM} , $\{[Ni(azpy)(pdia)(H_2O)] \cdot 0.5DCM\}$. *Synthesis.* The activated closed framework (**sqf-(azpy)(pdia)-Ni- β**) was soaked in dichloromethane (DCM) for 1 day to yield **sqf-(azpy)(pdia)-Ni- α_{DCM}** .

sqf-(azpy)(pdia)-Ni- α_{PX} , $\{[Ni(azpy)(pdia)(H_2O)] \cdot 0.5PX\}$. *Synthesis.* The activated closed framework (**sqf-(azpy)(pdia)-Ni- β**) was soaked in *para*-xylene (PX) for 1 day to yield **sqf-(azpy)(pdia)-Ni- α_{PX}** .

sqf-(azpy)(pdia)-Ni- α_{EB} , $\{[Ni(azpy)(pdia)(H_2O)] \cdot 0.58407EB\}$. *Synthesis.* The activated closed framework (**sqf-(azpy)(pdia)-Ni- β**) was soaked in ethylbenzene (EB) for 1 day to yield **sqf-(azpy)(pdia)-Ni- α_{EB}** .

DYNAMIC VAPOR SORPTION (DVS) EXPERIMENTS

Dynamic water vapor sorption studies were performed on ca. 10 mg samples using a Surface Measurement Systems Adventure Dynamic Vapor Sorption (DVS) system, which gravimetrically measures the uptake and loss of vapor using air as a carrier gas. Pure water was used as the adsorbate for these measurements, and temperature was maintained at 298 K by enclosing the system in a temperature-controlled incubator. The mass of the sample was determined by comparison to an empty reference pan and recorded by a high-resolution microbalance with a precision of 0.01 μ g. Sorption isotherms were measured from 0 to 95% relative humidity (RH) stepwise with a convergence equilibrium criterion $dm/dt = 0.01\%/min$. The minimum and maximum equilibration times for each step were 10 and 360 min, respectively.

RESULTS AND DISCUSSION

Single crystals of **sqf-(azpy)(pdia)-Ni** were obtained by solvothermal reaction of H_2pdia and *azpy* in DMF and water at 105 °C, yielding **sqf-(azpy)(pdia)-Ni- α_{DMF}** . Single-crystal

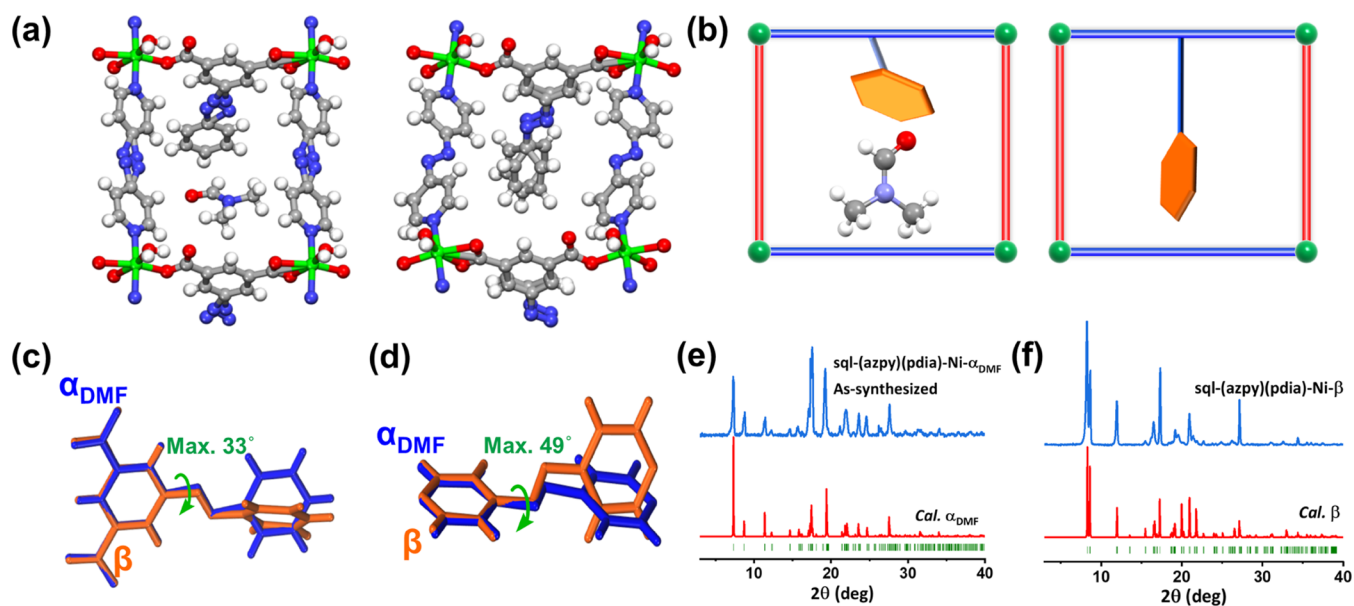


Figure 2. (a) sql nets in the α_{DMF} and β phases of sql-(azpy)(pdia)-Ni. (b) Schematic diagram of α_{DMF} and β . Superposed representations of deformations in (c) pdia^{2-} and (d) azpy in α_{DMF} (blue) and β (orange). Comparison of experimental PXRD patterns of (e) α_{DMF} and (f) β and PXRD patterns calculated from the SCXRD determined structures.

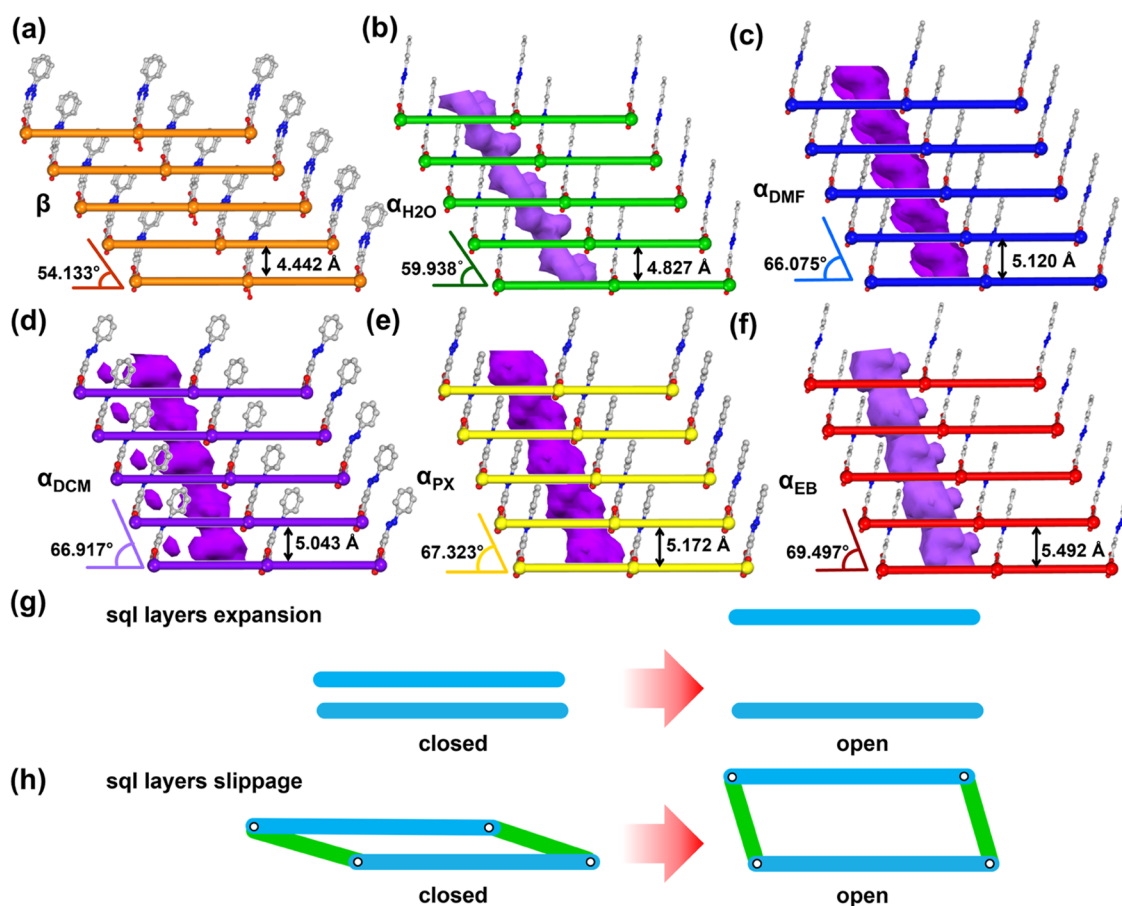


Figure 3. Schematic representation of the slippage and expansion of layers (rods = azpy linkers, balls = Ni^{2+} cations) and voids (purple channels) in the phases of sql-(azpy)(pdia)-Ni studied herein: (a) sql-(azpy)(pdia)-Ni- β (nonporous); (b) sql-(azpy)(pdia)-Ni- $\alpha_{\text{H}_2\text{O}}$; (c) sql-(azpy)(pdia)-Ni- α_{DMF} ; (d) sql-(azpy)(pdia)-Ni- α_{DCM} ; (e) sql-(azpy)(pdia)-Ni- α_{PX} ; and (f) sql-(azpy)(pdia)-Ni- α_{EB} . The mechanism of (g) sql layer expansion in previously reported sql networks and (h) sql layer slippage/expansion seen herein (sql layers = blue, hydrogen bonds = green).

X-ray diffraction (SCXRD) was used to determine the crystal structure of sql-(azpy)(pdia)-Ni- α_{DMF} , which had crystallized

in the monoclinic space group Pc with $a = 13.2072(4)$ Å, $b = 10.1554(3)$ Å, $c = 11.2001(4)$ Å, $\alpha = \gamma = 90^\circ$, $\beta =$

113.920(10)°, and $V = 1373.19(8) \text{ \AA}^3$ (Table S2). The octahedral mononuclear molecular building block (MBB)⁴⁶ is comprised of a Ni²⁺ cation coordinated to two N-donor atoms (N1 and N4) from two azpy ligands, three carboxylate O-donor atoms (O1, O3, and O4) from two pdia²⁻ ligands, and one O-donor atom (O5) from an aqua ligand. The formula is [Ni(pdia)(azpy)(H₂O)]·DMF (Figure S3). Hydrogen bonds were observed between each coordinated aqua molecule and O-atoms of coordinated pdia²⁻ ligands, both within individual sql layers (O...O = 2.614(5) Å) and between neighboring sql layers (O...O = 2.783(6) Å, Table S3). A 3D network with primitive cubic, pcu, topology structure results. The perpendicular distance between adjacent sql planes formed by Ni cations is 5.120(6) Å, and the dihedral angle between the sql plane and the plane of the parallelogram formed from two pairs of Ni²⁺ cations from adjacent sql layers is 66.075(13)° (Table S3). sql-(azpy)(pdia)-Ni- α_{DMF} has an effective pore size of ca. $6 \times 7 \text{ \AA}^2$ along the *c*-axis, and the calculated guest-accessible void volume is 19.5% (Figures 1c, S4, and S5). The bulk experimental powder X-ray diffraction (PXRD) pattern of α_{DMF} is consistent with that calculated from SCXRD data (Figure 2e).

Prior to conducting gas sorption experiments, sql-(azpy)(pdia)-Ni- α_{DMF} was soaked in methanol, exchanged twice daily for 2 days, and then activated at 100 °C under vacuum. The activated phase had transformed to a nonporous phase, sql-(azpy)(pdia)-Ni- β , as determined by SCXRD. sql-(azpy)(pdia)-Ni- β is a contorted version of sql-(azpy)(pdia)-Ni- α_{DMF} with the same connectivity and space group but different unit-cell parameters and a 14.6% reduction in unit-cell volume when compared to α_{DMF} (Table S2). The α_{DMF} to β transformation was accompanied by a folding motion of the channels along the *c*-axis, resulting in reduction of guest-accessible volume from 19.5% (α_{DMF}) to 0% (β) as calculated by Mercury software (Figure S4). The transformation from α_{DMF} and β can be attributed to a deformation in the pdia²⁻ and azpy ligands whereby “hinge-like” rotation occurred along the azo bond. In effect, the azo bonds in pdia²⁻ and azpy act as axles (Figure 2a,b). Close contacts in β were found between two interlayer pdia²⁻ linkers, which drives the change of α_{DMF} to a denser phase on guest removal (Figure S6, $d_{\text{C21A...N6}} = 3.42 \text{ \AA}$, $d_{\text{C20A...N5}} = 3.43 \text{ \AA}$). The dihedral angles of the isophthalate ring and phenyl ring of pdia²⁻ ligand in α_{DMF} and β changed substantially from 8.161 to 48.930° (47.373°) (Table S4). The azo bond, which connects the two pyridine rings in azpy ligand, also changes orientation during the transformation from α_{DMF} to β , the dihedral angles between these two pyridine rings being 4.756 and 69.133°, for α_{DMF} and β , respectively (Table S4).

When the isophthalate rings of pdia²⁻ in α_{DMF} and β are superposed and compared, the maximum torsional angle about the azo bond is ca. 33° (Figure 2c). Upon superposing the corresponding pyridine rings of azpy in α_{DMF} and β , the torsional angle about the azo bond was found to be ca. 49° (Figure 2d). These two rotations work synergistically to shrink the voids in β and are enabled by the pendant pdia²⁻ ligand (Figures 2a,b). The experimental PXRD pattern of β is consistent with that calculated from SCXRD data (Figure 2f). The interlayer H-bond between α_{DMF} and β hardly changed (2.783(6)–2.832(7) Å), but the distance between adjacent sql planes in α_{DMF} and β decreased from 5.120(6) to 4.442(10) Å (Figure 3c,a). The dihedral angle between the sql plane and the parallelogram formed by pairs of Ni²⁺ cations from

adjacent layers reduced from 66.075(13) to 54.133(21)° (Table S3). In effect, slippage between sql layers had occurred during the transformation from α_{DMF} to β .

To further explore the mechanism of flexibility in sql-(azpy)(pdia)-Ni, crystals of sql-(azpy)(pdia)-Ni- β were soaked in the following solvents: H₂O, DCM, PX, and EB. SCXRD experiments revealed that four additional open phases were obtained, namely, sql-(azpy)(pdia)-Ni- $\alpha_{\text{H}_2\text{O}}$, sql-(azpy)(pdia)-Ni- α_{DCM} , sql-(azpy)(pdia)-Ni- α_{PX} , and sql-(azpy)(pdia)-Ni- α_{EB} . SCXRD data revealed that folding/unfolding of the pores and slippage between layers had occurred in such a manner that sql-(azpy)(pdia)-Ni, in effect, adapts its structure for each guest. Cell volumes were as follows: $\beta = 1199.07(12) \text{ \AA}^3$; $\alpha_{\text{H}_2\text{O}} = 1296.43(5) \text{ \AA}^3$; $\alpha_{\text{DCM}} = 1350.30(7) \text{ \AA}^3$; $\alpha_{\text{DMF}} = 1373.19(8) \text{ \AA}^3$; $\alpha_{\text{PX}} = 1389.00(9) \text{ \AA}^3$; and $\alpha_{\text{EB}} = 1469.2(3) \text{ \AA}^3$ (Table S2). These cell volumes correspond to the relative molecular volume of each guest: H₂O ($2 \times 18.4 \text{ \AA}^3$); DCM ($1 \times 58 \text{ \AA}^3$); DMF ($1 \times 72.3 \text{ \AA}^3$); PX ($1 \times 110.2 \text{ \AA}^3$); and EB ($1 \times 110.2 \text{ \AA}^3$), as calculated by XSeed,⁴⁷ except for H₂O, which was calculated from the CSD.^{48,49} Although PX and EB exhibit the same molecular volume, the shape of PX enabled a better fit than EB, which in turn required a larger pore volume. Short contact distances between guest molecules and pore walls were observed for α_{DMF} ($d_{\text{(O...H)}} = 2.516 \text{ \AA}$), $\alpha_{\text{H}_2\text{O}}$ ($d_{\text{(O...O)}} = 2.969 \text{ \AA}$), α_{EB} ($d_{\text{(C-H...}\pi)} = 3.005 \text{ \AA}$), α_{DCM} ($d_{\text{(O...H)}} = 2.294 \text{ \AA}$), and α_{PX} ($d_{\text{(O...H)}} = 2.927 \text{ \AA}$) (Table S3). Disorder of ligands was observed in α_{DMF} , β , $\alpha_{\text{H}_2\text{O}}$, and α_{EB} related to host–guest interactions and framework flexibility. Overall, the analysis of the crystal structures of the six phases indicates that adaptive binding (Figures 3a–f and S5) and slippage motion are enabled by the pendant phenyldiazenyl moiety of the pdia²⁻ ligand.

The continuous nature of the slippage/expansion in sql-(azpy)(pdia)-Ni can be quantified by the sql layer separation and dihedral angle formed by the sql plane and the plane formed by pairs of Ni²⁺ cations from adjacent sql layers (Table S3). At one extreme, α_{EB} possesses the biggest void volume (21.8%), longest interlayer distance (5.492(15) Å), and most obtuse dihedral angle (69.497(20)°) (Figure 3f). At the other extreme, β is nonporous (0%) and has the shortest interlayer distance (4.442(10) Å) and the most acute dihedral angle (54.133(26)°) (Figure 3a). The interlayer hydrogen bonds in all six phases lie within a narrow range, 2.74(8)–2.83(7) Å (Table S3), whereas the other structural parameters are intermediate between the extremes. The motion between sql layers can be described as being analogous to parallel motion linkage, a concept from engineering and architecture (Figure 3h).⁵⁰

Layer expansion in previously reported sql networks like ELM-11,³⁶ ELM-12,⁵¹ and sql-1-Co-NCS¹⁷ resulted from phase transformations between two or more discrete phases (Figure 3g). In ELM-11, the expansion of sql layers was induced by carbon dioxide (CO₂),³⁶ *n*-butane,⁵² and acetylene (C₂H₂).⁵³ With increasing pressure of CO₂, the phase change from closed to open phases resulted in distances between sql layers of 4.427, 5.676, 5.685, and 6.960 Å. In ELM-12, vacuum heating prompted interlayer sql distances to decrease from 7.2 to 6.7 Å and then to 5.9 Å, corresponding to three distinct phases. C8 aromatics were reported to induce sql-1-Co-NCS to exhibit four distinct phases with interlayer sql distances of 4.46 (closed) to 9.15 (PX), 9.21 (*meta*-xylene, MX), 9.26 (*ortho*-xylene, OX), and 6.25 (EB) Å. In contrast, anchored by

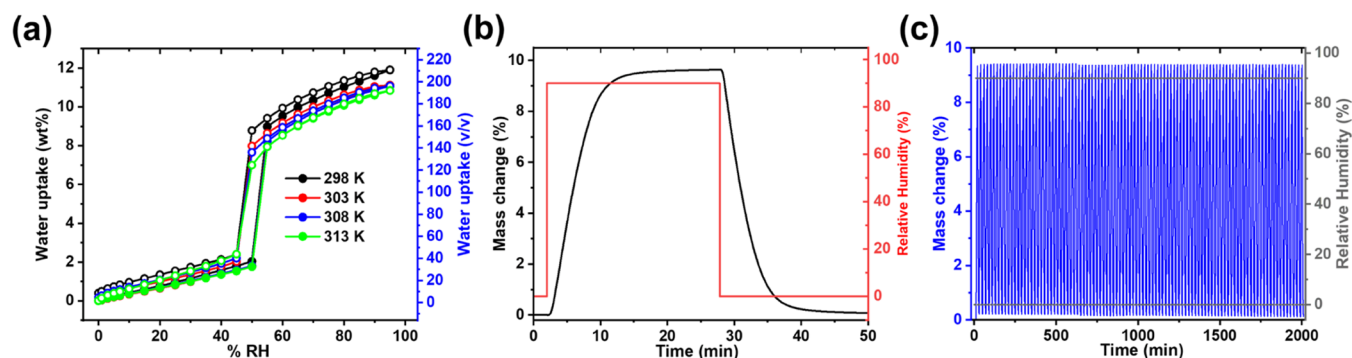


Figure 4. (a) Dynamic water vapor sorption isotherms of **sql-(azpy)(pdia)-Ni** at different temperatures (298, 303, 308, and 313 K). (b) Dynamic water vapor adsorption–desorption kinetic curves of **sql-(azpy)(pdia)-Ni** on 10.6 mg of sample at 298 K. (c) 100 cycles of dynamic adsorption–desorption water sorption of **sql-(azpy)(pdia)-Ni** between 0 and 90% RH on 10.4 mg of sample at 298 K.

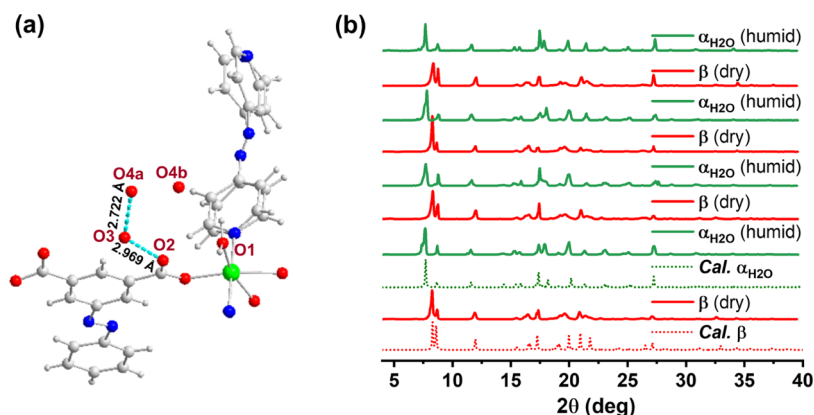


Figure 5. (a) Close contacts (cyan lines) between water molecules and ligand H_2pdia in **sql-(azpy)(pdia)-Ni- α_{H_2O}** . (b) Overlaid PXRD patterns showing the reversible change between **sql-(azpy)(pdia)-Ni- α_{H_2O}** and **sql-(azpy)(pdia)-Ni- β** under humidity swing conditions.

an interlayer H-bond, layer expansion was not as substantial in **sql-(azpy)(pdia)-Ni**. Rather, slippage of **sql** layers was induced by a series of guests to increase molecular volume (Figure 3h) accompanied by phase transformations driven by guest size.

The bulk phase purities of β and the five solvates reported herein were confirmed by matching of experimental and calculated PXRD patterns (Figures 2e,f and S7). Further, PXRD experiments conducted after immersing **sql-(azpy)(pdia)-Ni- β** in aqueous solutions with a range of pH values revealed that **sql-(azpy)(pdia)-Ni** retained its crystallinity after exposure to pH values ranging from 2 to 11 (Figure S8). Crystallinity was also retained under accelerated humidity stability testing conditions over 48 h (45 °C, 95% relative humidity, RH, Figure S9). The thermal stability of **sql-(azpy)(pdia)-Ni** was evaluated by thermogravimetric analysis (TGA) and variable temperature PXRD (VT-PXRD). TGA results revealed that **sql-(azpy)(pdia)-Ni- α_{DMF}** exhibited a mass loss of 11.4% at 115 °C, corresponding to one DMF molecule per formula unit (calculated 12.1%). TGA conducted on **sql-(azpy)(pdia)-Ni- β** showed no mass loss below thermal decomposition at 513 K (Figure S10). Attempts to analyze α_{H_2O} by TGA showed identical results to β , which indicated desorption of water at ambient conditions (indoor humidity < 40%, Figure S10). VT-PXRD conducted on **sql-(azpy)(pdia)-Ni- α_{H_2O}** revealed that a transformation to β occurred at 298 K at the onset of nitrogen (N_2) flow without application of heat, following which β was found to be stable up to 473 K (Figure S11).

Encouraged by the stability and responsive solution-phase uptake behavior of **sql-(azpy)(pdia)-Ni**, we studied its gas sorption properties. **sql-(azpy)(pdia)-Ni- β** revealed negligible uptake for N_2 at 77 K, whereas a stepped isotherm was observed for CO_2 at 195 K, with the inflection occurring at very low pressure ($P/P_0 = 0.01$, uptake $76 \text{ cm}^3/\text{g}$, Figure S12), confirming that **sql-(azpy)(pdia)-Ni** acts as a stimulus-responsive sorbent. In addition, the CO_2 sorption at 273 K exhibited the onset of a step at 681 mmHg, which is consistent with a structural transformation (Figure S12). This step was not observed below 1 bar at 298 K. The single point pore volume calculated at saturation ($P/P_0 = 0.9$) from the 195 K CO_2 isotherm is $0.118 \text{ cm}^3 \text{ g}^{-1}$, which agrees well with the crystallographically determined accessible void volume in **sql-(azpy)(pdia)-Ni- α_{H_2O}** ($0.124 \text{ cm}^3/\text{g}$), indicating that the CO_2 -included phase resembles α_{H_2O} .

That water can serve as a guest in **sql-(azpy)(pdia)-Ni** is of topical interest since water sorbents are being studied for their potential utility in water harvesting and dehumidification.^{54,55} To evaluate the sorption characteristics of **sql-(azpy)(pdia)-Ni**, dynamic water vapor sorption experiments were conducted on **sql-(azpy)(pdia)-Ni- β** . A stepped isotherm with an abrupt uptake was observed at 298 K. The step occurred between 50 and 55% RH with an uptake of 2 wt % ($36 \text{ cm}^3/\text{cm}^3$, cc/cc) at 50% RH and an uptake of 9 wt % (162 cc/cc) at 55% RH. The uptake difference of 7 wt % (126 cc/cc) is consistent with two water molecules per formula unit (6.8 wt %, Figure 4a). This value is in agreement with the observation of two water

molecules (O3 is fully occupied, while O4 is disordered over two positions; O4a/O4b is 0.43:0.57) in the crystal structure of **sql-(azpy)(pdia)-Ni- $\alpha_{\text{H}_2\text{O}}$** , which exhibits both water–water and water–framework short contacts (Figure 5a). Including the contribution from surface uptake, the saturation water uptake at 95% RH was found to be 12 wt % (216 cc/cc, Figure 4a).

In contrast to the pore filling (Type V) mechanism, which is often observed in rigid sorbent frameworks, such a stepped isotherm, along with the aforementioned structural changes, indicates that a nonporous-to-porous switching event occurs from β to $\alpha_{\text{H}_2\text{O}}$ during the adsorption of water. The desorption isotherm shows little hysteresis with steep water desorption at ca. 45% RH (Figure 4a). This kind of stepped sorption isotherm wherein the adsorption and desorption branches are centered between 40 and 60% RH range, but with distinct gate-opening and gate-closing partial pressures, is ideal for an autonomous moisture-controlled swing process.^{55–59} Moreover, upon increasing the sorption temperature from 298 to 303, 308, and 313 K, the relative gate-opening pressure hardly changed, and there was little loss of working capacity (313 K uptake of 11 wt % or 198 cc/cc), suggesting a wide operating temperature range for indoor humidity control.

The sorption kinetics of **sql-(azpy)(pdia)-Ni- β** were studied by subjecting a sample to humidity swing conditions, wherein RH was varied between 0 to 90%. As shown in Figure 4b, **sql-(azpy)(pdia)-Ni** can not only rapidly capture water vapor from the gas phase (as much as 9.4 wt % in 10 min or 169.2 cc/cc at 90% RH and 298 K) but also can be fully regenerated in less than 10 min once the RH is decreased to 0%. To evaluate the reusability of **sql-(azpy)(pdia)-Ni** for water sorption, humidity swing conditions of 298 K, 0–90% RH were applied to the sample for 100 cycles of 20 min each (10 min adsorption, 10 min desorption). No loss of working capacity was observed over the course of the experiment despite undergoing structural transformations during each cycle (Figure 4c). The recovered β phase retained crystallinity after the 100th cycle, as confirmed by PXRD analysis (Figure S13). To approximate real-world dehumidification conditions, sorption kinetics from 40 to 60% were also studied. The uptake was found to reach 9 wt % (162 cc/cc) within 60 min at 60% RH, and desorption to a loading of 1 wt % (18 cc/cc) occurred within 25 min at 40% RH. Working capacity was not significantly reduced over 12 cycles under these conditions (Figure S14).

The mechanism of water sorption by the switching of **sql-(azpy)(pdia)-Ni** was further studied by monitoring its structure by PXRD during repeated exposure to dry and humid conditions. First, **sql-(azpy)(pdia)-Ni** was exposed to dry N_2 flow at room temperature (10 min), exhibiting a PXRD pattern matching with the β phase. Then, instead of N_2 flow, a PXRD pattern of **sql-(azpy)(pdia)-Ni** was measured in a humid atmosphere at the same temperature. $\alpha_{\text{H}_2\text{O}}$ was obtained, as expected. PXRD patterns corresponded to the β and $\alpha_{\text{H}_2\text{O}}$ phases without loss of crystallinity over 4 cycles of the experiment (Figure 5b). In addition, single crystals randomly taken from a bulk sample of **sql-(azpy)(pdia)-Ni- β** and exposed to successive hydration and evacuation showed corresponding changes from β to $\alpha_{\text{H}_2\text{O}}$ and back to β did not exhibit signs of fragmentation despite somewhat diminished crystal quality (Table S2). Time-lapse spectra Fourier

Transform Infrared (FTIR) studies support the observed fast kinetics of water loading and unloading, showing a progressive reduction of the strong O–H water stretching peak at 3326 cm^{-1} until its disappearance within 10 min under ambient conditions (20 °C, 40% RH, Figure S15), leaving only peaks due to coordinated water in β (3356 cm^{-1}). These data reveal that regeneration of **sql-(azpy)(pdia)-Ni** can be easily realized by simply adjusting RH. Favorable intrinsic heat management arising from the endothermic structural transformation from β to $\alpha_{\text{H}_2\text{O}}$ is anticipated. To date, over 370 desiccant MOMs have been investigated, but fewer than 10% exhibit water-induced flexibility (Table S5), and, to our knowledge, no two-dimensional (2D) FMOMs have previously been studied for humidity control. **sql-(azpy)(pdia)-Ni** is therefore a potential candidate for indoor humidity control.

CONCLUSIONS

In conclusion, a new switching 2D MOF **sql-(azpy)(pdia)-Ni** was synthesized using the azpy and pendant-bearing pdia^{2-} ligands. Adaptive binding of guest molecules resulted in six distinct phases of **sql-(azpy)(pdia)-Ni** corresponding to phases loaded with DMF, H_2O , DCM, PX, EB, and a nonporous phase, as elucidated by SCXRD and PXRD. The continuum of phases exhibited by **sql-(azpy)(pdia)-Ni** was facilitated by the pendant phenyldiazenyl moiety on the pdia^{2-} ligand and interlayer hydrogen bonds between adjacent **sql** layers. This elastic-like motion is key to regulating access to the pores in each phase and was also observed during gas and H_2O sorption. In particular, the stepped water sorption isotherm with inflections in the range 40–60% RH makes **sql-(azpy)(pdia)-Ni** a potential candidate for indoor humidity control applications. Studies of stability and kinetics on **sql-(azpy)(pdia)-Ni** show excellent recyclability and retention of crystallinity. We attribute the elastic-like properties of **sql-(azpy)(pdia)-Ni** to the characteristic of rotation in diazo moieties and the pendant nature of one of the linker ligands, which enables a hinge-like mechanism of structural transformation. The amenability of **sql** nets to crystal engineering approaches will likely afford more members of this family of switching sorbent materials.

ASSOCIATED CONTENT

Supporting Information

The Supporting Information is available free of charge at <https://pubs.acs.org/doi/10.1021/acs.chemmater.2c03662>.

Materials and methods; supporting figures; supporting tables; and supporting references (PDF)

X-ray data for **sql-(azpy)(pdia)-Ni- α_{DMF}** (CIF)

X-ray data for **sql-(azpy)(pdia)-Ni- β** (CIF)

X-ray data for **sql-(azpy)(pdia)-Ni- β'** (CIF)

X-ray data for **sql-(azpy)(pdia)-Ni- α_{DCM}** (CIF)

X-ray data for **sql-(azpy)(pdia)-Ni- $\alpha_{\text{H}_2\text{O}}$** (CIF)

X-ray data for **sql-(azpy)(pdia)-Ni- α_{PX}** (CIF)

X-ray data for **sql-(azpy)(pdia)-Ni- α_{EB}** (CIF)

AUTHOR INFORMATION

Corresponding Author

Michael J. Zaworotko – Department of Chemical Science, Bernal Institute, University of Limerick, Limerick V94 T9PX, Republic of Ireland; orcid.org/0000-0002-1360-540X; Email: Michael.Zaworotko@ul.ie

Authors

Xia Li – Department of Chemical Science, Bernal Institute, University of Limerick, Limerick V94 T9PX, Republic of Ireland

Debobroto Sensharma – Department of Chemical Science, Bernal Institute, University of Limerick, Limerick V94 T9PX, Republic of Ireland; orcid.org/0000-0002-4918-0730

Varvara I. Nikolayenko – Department of Chemical Science, Bernal Institute, University of Limerick, Limerick V94 T9PX, Republic of Ireland

Shaza Darwish – Department of Chemical Science, Bernal Institute, University of Limerick, Limerick V94 T9PX, Republic of Ireland; orcid.org/0000-0001-9397-6886

Andrey A. Bezrukov – Department of Chemical Science, Bernal Institute, University of Limerick, Limerick V94 T9PX, Republic of Ireland

Naveen Kumar – Department of Chemical Science, Bernal Institute, University of Limerick, Limerick V94 T9PX, Republic of Ireland

Wansheng Liu – College of Chemistry, Nankai University, Tianjin 300071, People's Republic of China

Xiang-Jing Kong – Department of Chemical Science, Bernal Institute, University of Limerick, Limerick V94 T9PX, Republic of Ireland; orcid.org/0000-0003-2940-8600

Zhenjie Zhang – College of Chemistry, Nankai University, Tianjin 300071, People's Republic of China; orcid.org/0000-0003-2053-3771

Complete contact information is available at:

<https://pubs.acs.org/10.1021/acs.chemmater.2c03662>

Author Contributions

The manuscript was written through contributions of all authors. All authors have given approval to the final version of the manuscript.

Funding

The authors gratefully acknowledge Science Foundation Ireland (SFI Awards 16/IA/4624 and 12/RC/2278_P2), the Irish Research Council (IRCLA/2019/167), and Molecule RnD Ltd. (CRA AQUASORB I-IV).

Notes

The authors declare no competing financial interest.

REFERENCES

- (1) Uemura, K.; Matsuda, R.; Kitagawa, S. Flexible Microporous Coordination Polymers. *J. Solid State Chem.* **2005**, *178*, 2420–2429.
- (2) Horike, S.; Shimomura, S.; Kitagawa, S. Soft Porous Crystals. *Nat. Chem.* **2009**, *1*, 695–704.
- (3) Férey, G.; Serre, C. Large Breathing Effects in Three-Dimensional Porous Hybrid Matter: Facts, Analyses, Rules and Consequences. *Chem. Soc. Rev.* **2009**, *38*, 1380–1399.
- (4) Schneemann, A.; Bon, V.; Schwedler, I.; Senkovska, I.; Kaskel, S.; Fischer, R. A. Flexible Metal-Organic Frameworks. *Chem. Soc. Rev.* **2014**, *43*, 6062–6096.
- (5) Behera, N.; Duan, J.; Jin, W.; Kitagawa, S. The Chemistry and Applications of Flexible Porous Coordination Polymers. *EnergyChem* **2021**, *3*, No. 100067.
- (6) Wang, S. Q.; Mukherjee, S.; Zaworotko, M. J. Spiers Memorial Lecture: Coordination Networks That Switch between Nonporous and Porous Structures: An Emerging Class of Soft Porous Crystals. *Faraday Discuss.* **2021**, *231*, 9–50.
- (7) Forrest, K. A.; Verma, G.; Ye, Y.; Ren, J.; Ma, S.; Pham, T.; Space, B. Methane Storage in Flexible and Dynamical Metal–Organic Frameworks. *Chem. Phys. Rev.* **2022**, *3*, No. 021308.
- (8) Nugent, P.; Giannopoulou, E. G.; Burd, S. D.; Elemento, O.; Giannopoulou, E. G.; Forrest, K.; Pham, T.; Ma, S.; Space, B.; Wojtas, L.; Eddaoudi, M.; Zaworotko, M. J. Porous Materials with Optimal Adsorption Thermodynamics and Kinetics for CO₂ Separation. *Nature* **2013**, *495*, 80–84.
- (9) Fu, M.; Wang, Y.; Wang, X.; Sun, D. Metal-Organic Framework Materials for Light Hydrocarbon Separation. *ChemPlusChem* **2021**, *86*, 387–395.
- (10) Cui, X.; Chen, K.; Xing, H.; Yang, Q.; Krishna, R.; Bao, Z.; Wu, H.; Zhou, W.; Dong, X.; Han, Y.; Li, B.; Ren, Q.; Zaworotko, M. J.; Chen, B. Pore Chemistry and Size Control in Hybrid Porous Materials for Acetylene Capture from Ethylene. *Science* **2016**, *353*, 141–144.
- (11) Liang, B.; Zhang, X.; Xie, Y.; Lin, R. B.; Krishna, R.; Cui, H.; Li, Z.; Shi, Y.; Wu, H.; Zhou, W.; Chen, B. An Ultramicroporous Metal-Organic Framework for High Sieving Separation of Propylene from Propane. *J. Am. Chem. Soc.* **2020**, *142*, 17795–17801.
- (12) Bloch, E. D.; Queen, W. L.; Krishna, R.; Zadrozny, J. M.; Brown, C. M.; Long, J. R. Hydrocarbon Separations in a Metal-Organic Framework with Open Iron(II) Coordination Sites. *Science* **2012**, *335*, 1606–1610.
- (13) He, T.; Kong, X. J.; Bian, Z. X.; Zhang, Y. Z.; Si, G. R.; Xie, L. H.; Wu, X. Q.; Huang, H.; Chang, Z.; Bu, X. H.; Zaworotko, M. J.; Nie, Z. R.; Li, J. R. Trace Removal of Benzene Vapour Using Double-Walled Metal–Dipyrazolate Frameworks. *Nat. Mater.* **2022**, *21*, 689–695.
- (14) Gu, Z. Y.; Yan, X. P. Metal-Organic Framework MIL-101 for High-Resolution Gaschromatographic Separation of Xylene Isomers and Ethylbenzene. *Angew. Chem., Int. Ed.* **2010**, *49*, 1477–1480.
- (15) Krause, S.; Bon, V.; Senkovska, I.; Stoeck, U.; Wallacher, D.; Többs, D. M.; Zander, S.; Pillai, R. S.; Maurin, G.; Coudert, F. X.; Kaskel, S. A Pressure-Amplifying Framework Material with Negative Gas Adsorption Transitions. *Nature* **2016**, *532*, 348–352.
- (16) Taylor, M. K.; Runčevski, T.; Oktawiec, J.; Gonzalez, M. I.; Siegelman, R. L.; Mason, J. A.; Ye, J.; Brown, C. M.; Long, J. R. Tuning the Adsorption-Induced Phase Change in the Flexible Metal-Organic Framework Co(Bdp). *J. Am. Chem. Soc.* **2016**, *138*, 15019–15026.
- (17) Wang, S. Q.; Mukherjee, S.; Patyk-Każmierczak, E.; Darwish, S.; Bajpai, A.; Yang, Q. Y.; Zaworotko, M. J. Highly Selective, High-Capacity Separation of o-Xylene from C8 Aromatics by a Switching Adsorbent Layered Material. *Angew. Chem.* **2019**, *131*, 6702–6706.
- (18) Kundu, T.; Wahiduzzaman, M.; Shah, B. B.; Maurin, G.; Zhao, D. Solvent-Induced Control over Breathing Behavior in Flexible Metal–Organic Frameworks for Natural-Gas Delivery. *Angew. Chem.* **2019**, *131*, 8157–8161.
- (19) Hazra, A.; Van Heerden, D. P.; Sanyal, S.; Lama, P.; Esterhuysen, C.; Barbour, L. J. CO₂-Induced Single-Crystal to Single-Crystal Transformations of an Interpenetrated Flexible MOF Explained by in Situ Crystallographic Analysis and Molecular Modeling. *Chem. Sci.* **2019**, *10*, 10018–10024.
- (20) Ghosh, S. K.; Zhang, J. P.; Kitagawa, S. Reversible Topochemical Transformation of a Soft Crystal of a Coordination Polymer. *Angew. Chem., Int. Ed.* **2007**, *46*, 7965–7968.
- (21) Bon, V.; Klein, N.; Senkovska, I.; Heerwig, A.; Getzschmann, J.; Wallacher, D.; Zizak, I.; Brzhezinska, M.; Mueller, U.; Kaskel, S. Exceptional Adsorption-Induced Cluster and Network Deformation in the Flexible Metal-Organic Framework DUT-8(Ni) Observed by in Situ X-Ray Diffraction and EXAFS. *Phys. Chem. Chem. Phys.* **2015**, *17*, 17471–17479.
- (22) Loiseau, T.; Serre, C.; Huguénard, C.; Fink, G.; Taulelle, F.; Henry, M.; Bataille, T.; Férey, G. A Rationale for the Large Breathing of the Porous Aluminum Terephthalate (MIL-53) Upon Hydration. *Chem. - Eur. J.* **2004**, *10*, 1373–1382.
- (23) Mason, J. A.; Oktawiec, J.; Taylor, M. K.; Hudson, M. R.; Rodriguez, J.; Bachman, J. E.; Gonzalez, M. I.; Cervellino, A.; Guagliardi, A.; Brown, C. M.; Llewellyn, P. L.; Masciocchi, N.; Long, J. R. Methane Storage in Flexible Metal-Organic Frameworks with Intrinsic Thermal Management. *Nature* **2015**, *527*, 357–361.

- (24) Steinfink, H.; Brunton, G. D. Crystal structure of erbium oxalate trihydrate. *Inorg. Chem.* **1970**, *9*, 2112–2115.
- (25) Gable, R. W.; Hoskins, B. F.; Robson, R. A New Type of Interpenetration Involving Enmeshed Independent Square Grid Sheets. The Structure of Diaquabis-(4,4'-Bipyridine)Zinc Hexafluoro-silicate. *J. Chem. Soc. Chem. Commun.* **1990**, *23*, 1677–1678.
- (26) Fujita, M.; Washizu, S.; Ogura, K.; Kwon, Y. J. Preparation, Clathration Ability, and Catalysis of a Two-Dimensional Square Network Material Composed of Cadmium(II) and 4, 4'-Bipyridine. *J. Am. Chem. Soc.* **1994**, *116*, 1151–1152.
- (27) O'Hearn, D. J.; Bajpai, A.; Zaworotko, M. J. The "Chemistree" of Porous Coordination Networks: Taxonomic Classification of Porous Solids to Guide Crystal Engineering Studies. *Small* **2021**, *17*, No. 2006351.
- (28) Biradha, K.; Mondai, A.; Moulton, B.; Zaworotko, M. J. Coexisting Covalent and Non-Covalent Planar Networks in the Crystal Structures of {[M(Bipy)₂(NO₃)₂]-Arene} (M = Ni, 1; Co, 2; Arene = Chlorobenzene, o-Dichlorobenzene, Benzene, Nitrobenzene, Toluene or Anisole). *F. J. Chem. Soc., Dalton Trans.* **2000**, *2*, 3837–3844.
- (29) Noro, S. I.; Kitaura, R.; Kondo, M.; Kitagawa, S.; Ishii, T.; Matsuzaka, H.; Yamashita, M. Framework Engineering by Anions and Porous Functionalities of Cu(II)/4,4'-Bpy Coordination Polymers. *J. Am. Chem. Soc.* **2002**, *124*, 2568–2583.
- (30) Kondo, A.; Noguchi, H.; Carlucci, L.; Proserpio, D. M.; Ciani, G.; Kajiro, H.; Ohba, T.; Kanoh, H.; Kaneko, K. Double-step gas sorption of a two-dimensional metal-organic framework. *J. Am. Chem. Soc.* **2007**, *129*, 12362–12363.
- (31) Blatov, V. A.; Shevchenko, A. P.; Proserpio, D. M. Applied Topological Analysis of Crystal Structures with the Program Package Topospro. *Cryst. Growth Des.* **2014**, *14*, 3576–3586.
- (32) Groom, C. R.; Bruno, I. J.; Lightfoot, M. P.; Ward, S. C. The Cambridge Structural Database. *Acta Crystallogr., Sect. B: Struct. Sci., Cryst. Eng. Mater.* **2016**, *72*, 171–179.
- (33) Kumar, N.; Wang, S. Q.; Mukherjee, S.; Bezrukov, A. A.; Patyk-Kazmierczak, E.; O'Nolan, D.; Kumar, A.; Yu, M. H.; Chang, Z.; Bu, X. H.; Zaworotko, M. J. Crystal Engineering of a Rectangular S_q Coordination Network to Enable Xylenes Selectivity over Ethylbenzene. *Chem. Sci.* **2020**, *11*, 6889–6895.
- (34) Li, D.; Kaneko, K. Hydrogen Bond-Regulated Microporous Nature of Copper Complex-Assembled Microcrystals. *Chem. Phys. Lett.* **2001**, *335*, 50–56.
- (35) Bon, V.; Senkovska, I.; Wallacher, D.; Heerwig, A.; Klein, N.; Zizak, I.; Feyerherm, R.; Dudzik, E.; Kaskel, S. In Situ Monitoring of Structural Changes during the Adsorption on Flexible Porous Coordination Polymers by X-Ray Powder Diffraction: Instrumentation and Experimental Results. *Microporous Mesoporous Mater.* **2014**, *188*, 190–195.
- (36) Hiraide, S.; Tanaka, H.; Ishikawa, N.; Miyahara, M. T. Intrinsic Thermal Management Capabilities of Flexible Metal-Organic Frameworks for Carbon Dioxide Separation and Capture. *ACS Appl. Mater. Interfaces* **2017**, *9*, 41066–41077.
- (37) Kanoh, H.; Kondo, A.; Noguchi, H.; Kajiro, H.; Tohdoh, A.; Hattori, Y.; Xu, W. C.; Inoue, M.; Sugiura, T.; Morita, K.; Tanaka, H.; Ohba, T.; Kaneko, K. Elastic Layer-Structured Metal Organic Frameworks (ELMs). *J. Colloid Interface Sci.* **2009**, *334*, 1–7.
- (38) Ichikawa, M.; Kondo, A.; Noguchi, H.; Kojima, N.; Ohba, T.; Kajiro, H.; Hattori, Y.; Kanoh, H. Double-Step Gate Phenomenon in CO₂ Sorption of an Elastic Layer-Structured MOF. *Langmuir* **2016**, *32*, 9722–9726.
- (39) Park, J.; Sun, L. B.; Chen, Y. P.; Perry, Z.; Zhou, H. C. Azobenzene-Functionalized Metal-Organic Polyhedra for the Optically Responsive Capture and Release of Guest Molecules. *Angew. Chem.* **2014**, *126*, S952–S956.
- (40) Baroncini, M.; D'Agostino, S.; Bergamini, G.; Ceroni, P.; Comotti, A.; Sozzani, P.; Bassanetti, I.; Grepioni, F.; Hernandez, T. M.; Silvi, S.; Venturi, M.; Credi, A. Photoinduced Reversible Switching of Porosity in Molecular Crystals Based on Star-Shaped Azobenzene Tetramers. *Nat. Chem.* **2015**, *7*, 634–640.
- (41) Lyndon, R.; Konstas, K.; Ladewig, B. P.; Southon, P. D.; Kepert, P. C. J.; Hill, M. R. Dynamic Photo-Switching in Metal-Organic Frameworks as a Route to Low-Energy Carbon Dioxide Capture and Release. *Angew. Chem., Int. Ed.* **2013**, *52*, 3695–3698.
- (42) Li, B. A Novel Metal-Organic Framework as a Heterogeneous Catalysis for the Solvent-Free Conversion of CO₂ and Epoxides into Cyclic Carbonate. *Inorg. Chem. Commun.* **2018**, *88*, S6–S9.
- (43) He, H.; Du, J.; Su, H.; Yuan, Y.; Song, Y.; Sun, F. Four New Metal-Organic Frameworks Based on Bi-, Tetra-, Penta-, and Hexa-Nuclear Clusters Derived from 5-(Phenyldiazenyl)Isophthalic Acid: Syntheses, Structures and Properties. *CrystEngComm* **2015**, *17*, 1201–1209.
- (44) Geng, K.; Yang, X.; Zhao, Y.; Cui, Y.; Ding, J.; Hou, H. Efficient Strategy for Investigating the Third-Order Nonlinear Optical (NLO) Properties of Solid-State Coordination Polymers. *Inorg. Chem.* **2022**, *61*, 12386–12395.
- (45) Halder, G. J.; Kepert, C. J.; Moubaraki, B.; Murray, K. S.; Cashion, J. D. Guest-Dependent Spin Crossover in a Nanoporous Molecular Framework Material. *Science* **2002**, *298*, 1762–1765.
- (46) Gardner, G. B.; Venkataraman, D.; Moore, J. S.; Lee, S. Spontaneous assembly of a hinged coordination network. *Nature* **1995**, *374*, 792–795.
- (47) Barbour, L. J. X-Seed 4: Updates to a Program for Small-Molecule Supramolecular Crystallography. *J. Appl. Crystallogr.* **2020**, *53*, 1141–1146.
- (48) Li, Y.; Gai, T.; Lin, Y.; Zhang, W.; Li, K.; Liu, Y.; Duan, Y.; Li, B.; Ding, J.; Li, J. Eight Cd(Ii) Coordination Polymers with Persistent Room-Temperature Phosphorescence: Intriguing Dual Emission and Time-Resolved Afterglow Modulation. *Inorg. Chem. Front.* **2020**, *7*, 777–785.
- (49) Dias, I. M.; Junior, H. C. S.; Costa, S. C.; Cardoso, C. M.; Cruz, A. G. B.; Santos, C. E. R.; Candela, D. R. S.; Soriano, S.; Marques, M. M.; Ferreira, G. B.; Guedes, G. P. Mononuclear Coordination Compounds Containing a Pyrazole-Based Ligand: Syntheses, Magnetism and Acetylcholinesterase Inhibition Assays. *J. Mol. Struct.* **2020**, *1205*, No. 127564.
- (50) Morley, F. V. Linkages. *Sci. Mon.* **1919**, *9*, 366–378.
- (51) Kondo, A.; Chinen, A.; Kajiro, H.; Nakagawa, T.; Kato, K.; Takata, M.; Hattori, Y.; Okino, F.; Ohba, T.; Kaneko, K.; Kanoh, H. Metal-Ion-Dependent Gas Sorptivity of Elastic Layer-Structured MOFs. *Chem. - Eur. J.* **2009**, *15*, 7549–7553.
- (52) Bon, V.; Kavooosi, N.; Senkovska, I.; Kaskel, S. Tolerance of Flexible MOFs toward Repeated Adsorption Stress. *ACS Appl. Mater. Interfaces* **2015**, *7*, 22292–22300.
- (53) Li, L.; Krishna, R.; Wang, Y.; Wang, X.; Yang, J.; Li, J. Flexible Metal-Organic Frameworks with Discriminatory Gate-Opening Effect for the Separation of Acetylene from Ethylene/Acetylene Mixtures. *Eur. J. Inorg. Chem.* **2016**, *2016*, 4457–4462.
- (54) Hyunho, K. K.; Yang, S.; Narayanan, S.; Kapustin, E. A.; Furukawa, H.; Umans, A. S.; Yaghi, O. M.; Wang, E. N. Powered by Natural Sunlight. *Science* **2017**, *434*, 430–434.
- (55) Towsif Abtab, S. M.; Alezi, D.; Bhatt, P. M.; Shkurenko, A.; Belmabkhout, Y.; Aggarwal, H.; Weseliński, ŁJ.; Alsdun, N.; Samin, U.; Hedhili, M. N.; Eddaoudi, M. Reticular Chemistry in Action: A Hydrolytically Stable MOF Capturing Twice Its Weight in Adsorbed Water. *Chem* **2018**, *4*, 94–105.
- (56) Arundel, A. V.; Sterling, E. M.; Biggin, J. H.; Sterling, T. D. Indirect Health Effects of Relative Humidity in Indoor Environments. *Environ. Health Perspect.* **1986**, *65*, 351–361.
- (57) Llewellyn, P. L.; Schüth, F.; Grillet, Y.; Rouquerol, F.; Rouquerol, J.; Unger, K. K. Water sorption on mesoporous aluminosilicate MCM-41. *Langmuir* **1995**, *11*, S74–S77.
- (58) Abdulhalim, R. G.; Bhatt, P. M.; Belmabkhout, Y.; Shkurenko, A.; Adil, K.; Barbour, L. J.; Eddaoudi, M. A Fine-Tuned Metal-Organic Framework for Autonomous Indoor Moisture Control. *J. Am. Chem. Soc.* **2017**, *139*, 10715–10722.
- (59) Zhu, N. X.; Wei, Z. W.; Chen, C. X.; Xiong, X. H.; Xiong, Y. Y.; Zeng, Z.; Wang, W.; Jiang, J. J.; Fan, Y. N.; Su, C. Y. High Water Adsorption MOFs with Optimized Pore-Nanospaces for Autonomous

Indoor Humidity Control and Pollutants Removal. *Angew. Chem., Int. Ed.* **2022**, *61*, No. e202112097.

Recommended by ACS

Pore Environmental Modification by Alkoxy Groups in Pore-Space-Partitioned Metal–Organic Frameworks to Achieve Gas Uptake-Selectivity Balance

Shu-Yi Li, Quan-Guo Zhai, *et al.*

APRIL 26, 2023

INORGANIC CHEMISTRY

READ 

Discovery of a Scalable Metal–Organic Framework with a Switchable Structure for Efficient CH₄/N₂ Separation

Miao Chang, Jian-Feng Chen, *et al.*

MAY 19, 2023

CHEMISTRY OF MATERIALS

READ 

Control over Phase Transformations in a Family of Flexible Double Diamondoid Coordination Networks through Linker Ligand Substitution

Kyriaki Koupepidou, Michael J. Zaworotko, *et al.*

APRIL 27, 2023

CHEMISTRY OF MATERIALS

READ 

Simultaneous Control of Flexibility and Rigidity in Pore-Space-Partitioned Metal–Organic Frameworks

Yuchen Xiao, Pingyun Feng, *et al.*

MAY 10, 2023

JOURNAL OF THE AMERICAN CHEMICAL SOCIETY

READ 

Get More Suggestions >